ACS OMEGA
http://pubs.acs.org/journal/acsodf
Article

DFT Study on Corrosion Inhibition by Tetrazole Derivatives: Investigation of the Substitution Effect

Marzieh Esmaeilzadeh Khabazi and Alireza Najafi Chermahini*

Cite This: ACS Omega 2023, 8, 9978–9994
Read Online

ABSTRACT: Corrosion is one of the problems that most industries face. Our aim in the current study is to perform density functional theory calculations and Monte Carlo simulation to theoretically investigate the corrosion inhibition of the copper (1 1 1) surface by tetrazole molecules and a group of their derivatives. These compounds have electron-donating groups (CH_3, CH_3O, and OH) and electron-withdrawing groups (F, CN, and NO_2). Two different isomeric forms of tetrazole molecules and their derivatives, including 1*H* and 2*H* tautomers, were studied in two configurations, parallel and perpendicular to the Cu (1 1 1) surface. With the help of DMol3 calculations, the most important parameters related to the molecular ability of tetrazole derivatives as corrosion inhibitors include the adsorption energy (ΔE), E_{HOMO}, E_{LUMO}, E_{gap}, and issues related to chemical reactions, including total hardness (η), electronegativity (χ), and electron fraction transitions from the anti-corrosion molecule to the copper atom (ΔN), were calculated and compared in the tetrazole molecules and their derivatives. Also, with the help of adsorption locator calculations, the inhibitory effects of these compounds were theoretically investigated in an acidic environment. Through these calculations, it was determined that tetrazole molecules with electron-donating groups adsorbed perpendicularly to the copper (1 1 1) surface, by forming a stronger bond, are considered suitable corrosion inhibitors. Also, among the examined molecules, the 2*H*-tetrazole isomer form plays a more influential role than the 1*H*-tetrazole form.

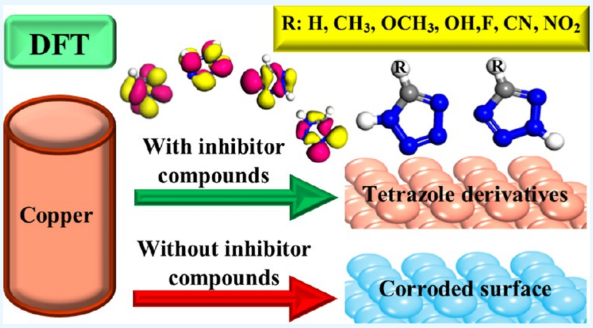

1. INTRODUCTION

The fifth most prevalent metal in the earth's crust and the oldest metal used by humanity is copper, which is used in the pure or alloyed form in various industries such as electronic industries, offshore industries, electrical plants, cooling towers, heat exchangers, and medicine. Among the properties of copper and its alloys, we can mention resistance to corrosion, good electrical and thermal conductance, mechanical performance, flexibility, and antimicrobial properties.[1,2] Corrosion is an electrochemical and natural process that occurs between the metal and its surrounding environment, in which the property of the metal changes. In terms of thermodynamics, corrosion products are at a lower energy level than metal. Therefore, the tendency to reach a lower energy level causes corrosion. Copper resists corrosion in the atmosphere by forming a protective oxide layer. Still, it is weak against corrosive agents such as nitrite, sulfate, and chloride ions, and pitting corrosion occurs. Moisture also plays a vital role in metal surface corrosion by providing electrolytes in cathodic and anodic processes. Among the factors affecting the corrosion rate are salts and impurities in the environment, which facilitate the exchange of electrons between materials involved in the corrosion process by creating an electrolyte. Also, in acidic environments, the speed of electrolyte formation and the corrosion rate is higher. Typically, copper structures are used in corrosive environments such as salt water that contains corrosive anions. Corrosion on the surface of copper and the formation of products resulting from it have adverse effects on the performance of systems made of copper and reduce their efficiency. Therefore, protecting copper metal against corrosion is an essential and practical issue.[3−5] Anti-corrosion compounds, especially organic molecules whose physicochemical properties can be modified by altering the substituents connected to their structure, are used to protect metals against corrosion. These compounds react with the metal surface and form a protective substrate to mitigate this phenomenon. The application of these molecules as an anti-corrosion agent and a deterrent is more cost-effective and convenient due to their easy preparation and efficiency compared with other techniques, such as self-healing methods

Received: November 8, 2022
Accepted: February 24, 2023
Published: March 8, 2023

or the application of corrosion-resistant alloys.[6,7] The copper atom has empty orbitals in the capacitive layer which makes its surface prone to corrosion. Therefore, electron-donating compounds should be used as anti-corrosion compounds on the copper surface.[8]

Among the organic molecules, azoles (five-membered heterocyclic comprising at least one nitrogen atom) are considered efficient corrosion inhibitors of metals.[9−15] Among azoles, tetrazoles with four nitrogen atoms in the ring are heavily investigated due to their attractive properties. Generally, tetrazoles exist in two tautomeric forms (1*H* and 2*H*, see Scheme 1), in which the 2*H*-form prevails in the gas phase, while the 1*H*-form is more stable in the liquid.[16] Also, while tetrazole rings are weak bases, by having a proton connected to the N1 or N2 position, they show strong acidic character in the range of carboxylic acids (pK_a ∼ 4.75).[17−19] Moreover, tetrazole derivatives are aromatic, and the structural parameters are considerably affected by the quiddity of the substituent in the ring.[20−22]

Scheme 1. Tautomerization in Tetrazoles

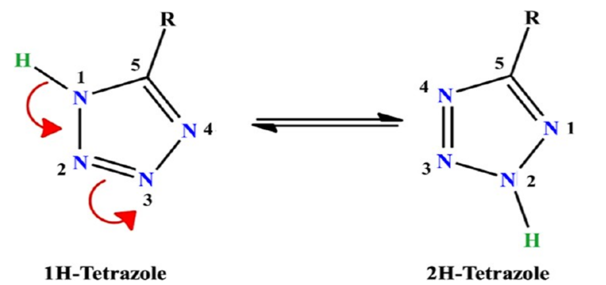

Due to their exciting properties, tetrazoles have been used in various applications such as explosive and propellant materials,[23] medicinal chemistry,[24] solar cells,[25,26] agriculture,[27,28] and anti-corrosion compounds.[29−35]

Recently, computational chemistry, as a fast, inexpensive, and reliable tool, has garnered interest in the investigation and evaluation of corrosion inhibitors' performance in different media and metal surfaces. Many documents have been published in the literature dealing with the mechanism and assessment of effective parameters of corrosion inhibitors on a molecular scale. In one study, four compounds, 1,2,3,4-tetrazole (TZ), 1-phenyl-1,2,3,4-tetrazole (PTZ), 5-amino-1,2,3,4-tetrazole (ATZ), and 1-phenyl-5-mercapto-1,2,3,4-tetrazole (PMTZ), were employes as anti-corrosion compounds of the copper (1 1 1) surface in the acidic condition. The outcomes of DFT calculations and Monte Carlo (MC) simulations show the following efficiency: TZ > ATZ > PTZ > PMTZ. The planar skeleton of these compounds, the electron clouds on the aromatic rings, and the presence of several lone pair electrons are the reasons for these results.[36] TAN et al. studied the inhibitory effect of 5-phenyl-tetrazole (PT), 5-(4-bromophenyl)-2*H*-tetrazole (5-4-BPT), and 5-(2-bromophenyl)-1*H*-tetrazole (5-2-BPT) on the surface of copper by experimental methods and DFT calculations. The order of corrosion inhibition performance according to practical and theoretical results was 5-4-BPT > 5-2-BPT > PT.[37] In another study, Chiter et al. performed DFT calculations on 2-mercapto-benzothiazole (MBT) as a corrosion suppressor for copper oxide surfaces. Analyses showed that MBT replaces OH and H_2O at the Cu_2O surface and forms a protective layer in the aqueous medium.[38] Also, Liu and co-workers studied the adsorption of 5-heteroaryl tetrazoles on copper surfaces using electrochemical measurement and DFT calculations. According to their results, corrosion inhibition is achieved through a charge transfer process.[39] Kovačević and Kokalj investigated DFT studies for azole molecules, including imidazole, 1,2,3-triazole, tetrazole, and pentazole on Cu (1 1 1) and Al (1 1 1) surfaces. According to this research, it was found that increasing the number of nitrogen atoms in the azole ring increases the electronegativity and chemical hardness. As the hardness of the inhibitor molecule increases, the hybridization with the metal surface becomes more difficult, and the bond between the inhibitor molecule and the phase surface decreases.

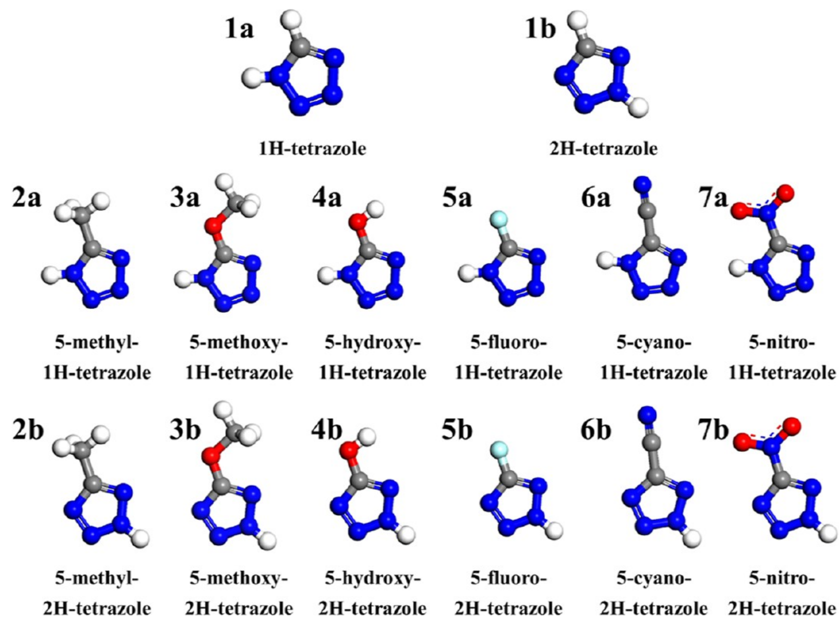

Figure 1. Optimized molecular structure of tetrazoles and their derivatives (atom legend: white = H, gray = C, blue = N, red = O, and light blue = F).

https://doi.org/10.1021/acsomega.2c07185
ACS Omega 2023, 8, 9978−9994

Table 1. Calculation of HOMO, LUMO Energies, and E_{gap} for Optimized Tetrazole Molecules and Their Derivatives and the Total Energy Difference of Each Tautomer before Adsorption

molecules	$\Delta E_{\text{total before adsorption}}$ (kcal/mol)	E_{HOMO} (eV)	E_{LUMO} (eV)	I (eV)	A (eV)	η (eV)	χ (eV)	σ (eV)	ΔN	E_{gap} (eV)
1a	0	−6.782	−1.725	6.782	1.725	2.528	4.253	0.395	0.136	5.057
1b	−3.1	−7.016	−2.024	7.016	2.024	2.496	4.520	0.400	0.085	4.992
2a	0	−6.538	−1.504	6.538	1.504	2.517	4.021	0.397	0.183	5.034
2b	−2.4	−6.762	−1.778	6.762	1.778	2.492	4.272	0.401	0.135	4.984
3a	0	−6.556	−1.345	6.556	1.345	2.605	3.950	0.383	0.191	5.211
3b	−2.1	−6.306	−1.81	6.306	1.81	2.248	4.058	0.444	0.197	4.496
4a	0	−6.803	−1.489	6.803	1.489	2.657	4.146	0.376	0.150	5.314
4b	−3.1	−6.607	−1.978	6.607	1.978	2.314	4.292	0.432	0.141	4.629
5a	0	−7.179	−2.001	7.179	2.001	2.589	4.590	0.386	0.068	5.178
5b	−2.2	−7.518	−2.435	7.518	2.435	2.541	4.976	0.393	−0.006	5.083
6a	0	−7.611	−3.373	7.611	3.373	2.110	5.492	0.471	−0.128	4.238
6b	−6.1	−7.838	−3.008	7.838	3.008	2.410	5.423	0.414	−0.098	4.830
7a	0	−7.704	−4.669	7.704	4.669	1.517	6.186	0.658	−0.408	3.035
7b	−0.2	−7.356	−4.146	7.356	4.146	1.600	5.751	0.623	−0.250	3.210

Therefore, imidazole with two N atoms showed the highest bond strength (0.69 eV) with the Cu (1 1 1) surface.[40] Kumar and his colleagues investigated the inhibition mechanisms of the copper surface by imidazole, adenine, purine, and 6-benzylamine purine (BPA) compounds. In this research, DFT and ReaxFF calculations were used. The optimization results showed the trend of BPA > adenine > purine > imidazole in corrosion inhibition. Also, the formation of a strong bond between surface Cu atoms and N inhibitor molecules was also proved.[41] In another study by Kumar et al., by using DFT and ReaxFF simulations, the synergistic effect between benzyl azide (BA) and butyn-1-ol (BOL) molecules on copper surface corrosion inhibition was checked out. Based on the calculation of interaction energy, they predicted the trend of BA−BOL > BA−BA > BOL−BOL on the Cu (1 1 1) surface. The reason for this synergism was reported as side interactions between N_{BA} and H_{BOL}.[42]

In this study, using density functional theory (DFT) calculations and MC simulation, we investigated the changes in the adsorption energy of tetrazole molecules and their derivatives on the copper surface and determined the most stable state. Also, by examining the Mulliken charge and the nucleophilic and electrophilic properties through the parameter of the Fukui function and comparing the density of states (DOS) diagrams with the single surface, the inhibitory effects of tetrazole molecules and different functional groups were investigated. According to previous work, substitution at the 5-position fundamentally changes the physicochemical properties of the tetrazole ring.[43−46] The studied compounds include 1*H*-tetrazole (**1a**), 2*H*-tetrazole (**1b**), 5-methyl-1*H*-tetrazole (**2a**), 5-methyl-2*H*-tetrazole (**2b**), 5-methoxy-1*H*-tetrazole (**3a**), 5-methoxy-2*H*-tetrazole (**3b**), 5-hydroxy-1*H*-tetrazole (**4a**), 5-hydroxy-2*H*-tetrazole (**4b**), 5-fluoro-1*H*-tetrazole (**5a**), 5-fluoro-2*H*-tetrazole (**5b**), 5-cyano-1*H*-tetrazole (**6a**), 5-cyano-2*H*-tetrazole (**6b**), 5-nitro-1*H*-tetrazole (**7a**), and 5-nitro-2*H*-tetrazole (**7b**), and their structures are shown in Figure 1.

2. COMPUTATIONAL METHODS

2.1. Quantum Chemical Calculations. DFT is one of the computational procedures in the field of science that has many applications in theoretical discussions.[47] For this project, the DMol3 package in Materials Studio version 2017 was used to perform DFT calculations. Geometric optimizations were executed based on the generalized gradient approximation (GGA) function and Perdew−Wang exchange (PW91) and using the OBS method for DFT-D correction. In the convergence tolerance, the relevant options were set as follows: quality = fine, energy = 1.0×10^{-5} Ha, max. force = 0.002 Ha/Å, max. displacement = 0.005 Å, max. interactions = 1000, and max. step size = 0.3 Å. The base settings DNP was set for effective core potentials and *k*-point 3 × 3 × 1. Options for quality of geometry, integration accuracy, and SCF tolerance were also set as fine. The smearing parameter was selected as 0.02 Ha. Also, max. SCF cycles were set to 1000 and multipolar expansion to octupole. To build the surface, a supercell 3 × 3 × 1 with a vacuum thickness of 20.00 Å was used.[48] The adsorption energy and binding energy of tetrazole molecules and their derivatives on the Cu (1 1 1) were calculated by eqs 1 and 2, respectively. Binding energy is the negative equivalent of adsorption energy.[36,49]

$$\Delta E_{\text{adsorption}} = E_{\text{total compound/Cu(1 1 1)}} - (E_{\text{total Cu (1 1 1)}} + E_{\text{total compound}}) \quad (1)$$

$$\Delta E_{\text{binding}} = -\Delta E_{\text{adsorption}} = (E_{\text{total Cu(1 1 1)}} + E_{\text{total compound}}) - E_{\text{total compound/Cu(1 1 1)}} \quad (2)$$

In these relations, $E_{\text{total compound/Cu (1 1 1)}}$ is the total energy of the adsorbed compound on the surface, $E_{\text{total Cu (1 1 1)}}$ is the total energy of the copper surface (1 1 1) alone, and $E_{\text{total compound}}$ is the total energy of the desired compound alone.[41,50]

2.2. MC Simulation. The interaction between tetrazole molecules and their derivatives with the Cu (1 1 1) surface was investigated through MC simulation. For this purpose, the adsorption locator module was used in Materials Studio software version 2017. Low energy configuration and energy distribution properties were calculated using a simulated annealing task, COMPASS force field, optimized geometry, and bounding box location settings. In the simulated annealing section, the number of cycles was set to 3, and the step per cycle was set to 15000. Also, in the optimized geometry section, the energy and force options were selected as 0.001 kcal/mol and 0.5 kcal/mol Å, respectively, and the

https://doi.org/10.1021/acsomega.2c07185
ACS Omega 2023, 8, 9978−9994

automated temperature control option was activated. In the summation method section, electrostatic was set on a group-based, and Van der Waals was set as atom-based. To check the solvent effect, 80 water molecules and 2 HCl molecules were loaded in the medium.[39,51−53]

3. RESULTS AND DISCUSSION

3.1. Quantum Chemical Calculations on Tetrazole Derivatives in the Gas Phase. One of the significant factors for recognizing the properties and effectiveness of a corrosion-inhibiting molecule is to study its electronic and spatial structures. For this purpose, quantum chemical calculations were performed for tetrazole molecules and their derivatives.[54]

According to calculations (Table 1) and in agreement with previously reported data,[16,55] tetrazole derivatives, 2*H*-forms, are more stable in the gas phase. For example, for the 5-cyanotetrazole, the 2*H*-form is more durable than 1*H* by −6.1 kcal/mol, while for the 5-nitrotetrazole, the 2*H*-form is more stable by −0.2 kcal/mol. It is clear that for electron-donating substituents, the energy difference between two tautomeric forms decreases. Also, Table 1 shows the energy values for HOMO (highest occupied molecular orbital), LUMO (lowest unoccupied molecular orbital), and E_{gap} (gap energy between HOMO and LUMO), and values of the E_{gap} were calculated using the following equation

$$E_{gap} = E_{LUMO} - E_{HOMO} \quad (3)$$

The values related to hardness (η), softness (σ), electronegativity (χ), and a fraction of transferred electrons (ΔN) for tetrazole molecules and their derivatives were calculated using the following relationships[56−59]

$$I = -E_{HOMO} \quad (4)$$

$$A = -E_{LUMO} \quad (5)$$

$$\eta = (I - A)/2 \quad (6)$$

$$\chi = (I + A)/2 \quad (7)$$

$$\sigma = 1/\eta \quad (8)$$

$$\Delta N = (\varnothing - \chi_{compound})/2\eta_{compound} \quad (9)$$

Using HOMO and LUMO energies and calculating the gap energy, the chemical reactivity of molecules with the metal surface could be determined. HOMO energy is related to the molecule's tendency to donate electrons, and LUMO energy determines the molecule's direction to accept electrons.[60] With the increase in HOMO energy, or in other words, decrease in E_{gap}, the capability of the molecule to form bonds with the metal surface increases.[41,61] Figure 2 shows the HOMO and LUMO plots of the optimized molecules, respectively. As Table 1 shows, in general, in tetrazole molecules in the 2*H*-form, E_{gap} values have decreased for all functional groups. In tetrazole molecules in the 1*H*-form, we see a decrease in the E_{gap} for the electron-withdrawing groups and an increase in the E_{gap} for the electron-donating groups. For example, it is predicted that the functional group OH in the form of 2*H*-tetrazole as an electron-donating group with a gap energy of 4.629 eV compared to the functional group of CN in the form of 2*H*-tetrazole as an electron-withdrawing group with the gap energy of 4.830 eV, could better control the corrosion of the metal surface. According to the calculated data, it can be concluded that in tetrazole molecules with electron-withdrawing functional groups, the distance between the HOMO and LUMO energy levels is shorter. Because of the negativity of ΔN values, the reaction with the surface through electron transfer from metal to the inhibitory molecule is carried out, which is an undesirable process for corrosion resistance.

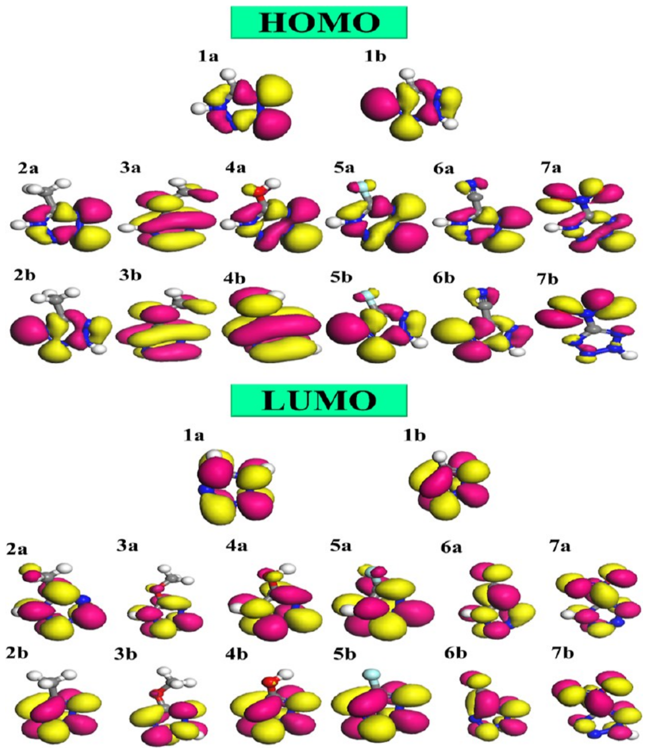

Figure 2. HOMO and LUMO plots of optimized tetrazoles and their derivatives.

Important geometrical parameters of tetrazole rings are presented in Table 2. A closer look at Table 2 indicates that bond lengths are affected by changing the substituent. For example, the 1*H* isomers of the tetrazole ring with NO_2, and CH_3O substituent N1−N2, and N1−C5 bond lengths are 1.345, 1.368, 1.349, and 1.352 Å, respectively.

One of the significant parameters in the scrutiny of anti-corrosion compounds is the calculation of hardness (η) and

Table 2. Important Geometrical Parameters of Tetrazole Derivatives

	N1−N2	N2−N3	N3−N4	N1−C5	N4−C5	N1−H	N2−H
1a	1.358	1.299	1.364	1.349	1.320	1.013	
1b	1.329	1.335	1.314	1.332	1.355		1.013
2a	1.359	1.298	1.362	1.353	1.325	1.015	
2b	1.333	1.336	1.313	1.338	1.363		1.014
3a	1.368	1.296	1.368	1.352	1.321	1.012	
3b	1.340	1.334	1.315	1.338	1.359		1.013
4a	1.370	1.296	1.367	1.347	1.318	1.013	
4b	1.339	1.333	1.318	1.355	1.355		1.013
5a	1.363	1.300	1.368	1.347	1.306	1.014	
5b	1.334	1.336	1.318	1.328	1.346		1.014
6a	1.348	1.302	1.350	1.360	1.334	1.015	
6b	1.324	1.344	1.305	1.343	1.367		1.014
7a	1.345	1.309	1.349	1.349	1.321	1.016	
7b	1.322	1.345	1.308	1.334	1.354		1.016

https://doi.org/10.1021/acsomega.2c07185
ACS Omega 2023, 8, 9978−9994

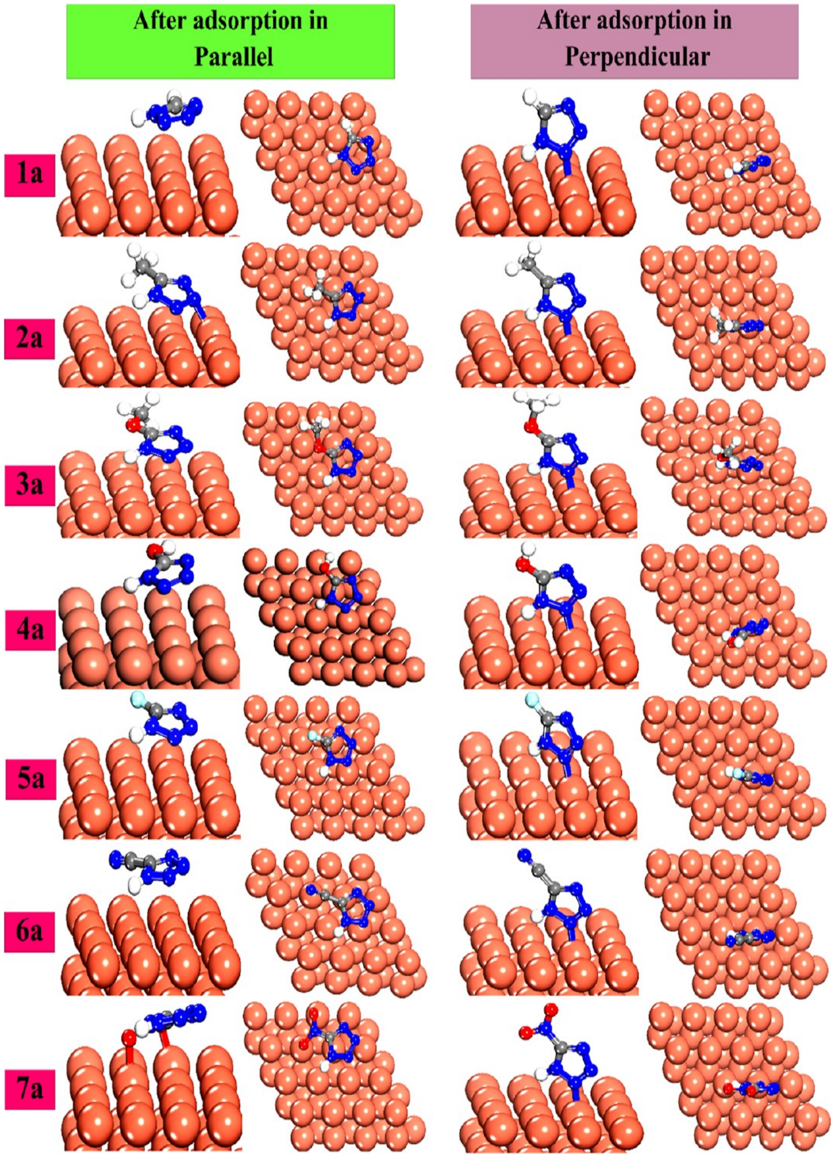

Figure 3. Optimal structures of 1*H*-form tetrazole molecules and their derivatives in parallel and perpendicular on the Cu (1 1 1).

softness (σ). The softer a combination is, the more reactive it is. The electronegativity (χ) index, also expresses the propensity of compounds to accept electrons in forming a back bond. These donation and back-donation processes strengthen the adsorption of the desired compound on the metal surface.[57] According to the data in Table 1, the softness values are higher for electron-donating groups. For example, in molecule **2a**, the σ is equivalent to 0.397 eV, and in molecule **6a**, it is equal to 0.471 eV. Therefore, the reactivity of the **6a** molecule with the copper surface is higher than that of the **2a** molecule. Also, with the incorporation of electron-withdrawing groups, the tendency to transfer electrons from the surface to the molecule increases, which harms protecting the surface against corrosion (χ: **1b** = 4.520, **4b** = 4.292, **7b** = 5.751; eV). The transferred electron fraction parameter describes how the surface reacts with the metal. If $\Delta N < 0$, it means that the electron has been moved from the surface to the molecule, and if $\Delta N > 0$, the electron has been transmissive from the molecule to the surface.[36] Ø is the work function in equation number 8, and its value for copper is 4.96 eV.[62]

The positive values of ΔN in the electron-donating groups (Table 1) indicate the transfer of electrons from tetrazole molecules to the surface of copper (1 1 1), while the negative values of ΔN in the electron-withdrawing groups (Table 1) are a confirmation of electron transfer from the surface of copper (1 1 1) to tetrazole molecules. The highest value of ΔN for **3b** = 0.197, and the lowest value for **7b** = −0.250. The higher the value of ΔN, the greater its effect in protecting the metal surface against corrosion.

3.2. DFT Calculations. Examining the process of adsorption of molecules on the surface by DFT gives us a better understanding of how corrosion is inhibited.[63] With the help of these calculations, the functions of Fukui can be determined, which determine the locations of nucleophilic and electrophilic attacks. According to Parr and Yang's theory, f_k^+ will have the maximum value in nucleophilic attacks and f_k^- in electrophilic attacks.[64,65] Another parameter considered in DFT calculations is the Mulliken charge. The higher the negative charge of an atom, the more it tends to react with the metal surface by giving it an electron.[66] Also, to understand the nature of the reaction between the surface and the

https://doi.org/10.1021/acsomega.2c07185
ACS Omega 2023, 8, 9978−9994

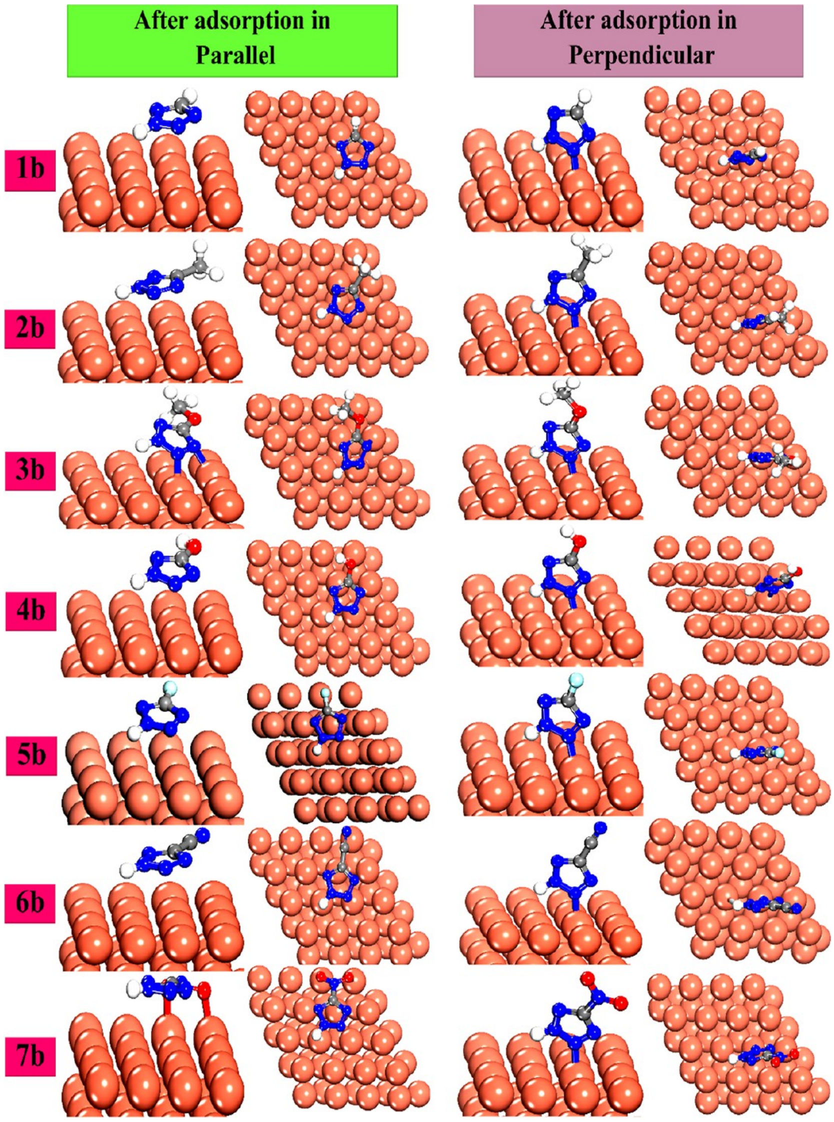

Figure 4. Optimal structures of 2*H*-form tetrazole molecules and their derivatives in parallel and perpendicular on the Cu (1 1 1).

corrosion inhibitor at the electron surface, the predicted DOS was investigated. After the inhibitory molecules are adsorbed by the metal surface, the partial DOS (PDOS) peaks become wider, indicating the hybridization of the molecule and metal orbitals. In general, by examining the PDOS diagrams, it can be said that before the adsorption of the corrosion inhibitor molecule, the peaks are sharper. After the adsorption, the broadening of the peaks can be seen, which is due to the hybridization of 2p-N with 3d-Cu.[67,68] The more substantial the interaction between the inhibitory molecule and the metal, the more effective it will be in preventing corrosion of the copper surface.[69,70] In this section, adsorption geometries parallel to and perpendicular to the copper surface (1 1 1) for tetrazole **1a** and **1b** molecules were investigated. Then, the electron-donating groups (CH_3, CH_3O, and OH) and the electron-withdrawing groups (F, CN, and NO_2) were replaced with hydrogen atoms attached to carbon, and their adsorption action was studied. Total adsorption energies, binding energies, Fukui functions, Mulliken charges, and PDOS diagrams were determined for each case. Figures 3 and 4 show the optimal structures of tetrazole molecules and their derivatives parallel and perpendicular to the copper surface (1 1 1).

3.2.1. Comparison of Total Adsorption Energies and Binding Energies. Although the exact function of organic molecules as corrosion inhibitors is unknown, it has been found that proper adsorption of inhibitor molecules on the surface is a valuable approach to achieve the desired effects in corrosion prevention. Information about the adsorption energy of tetrazole molecules and their derivatives is given in Table 3. As can be seen, the adsorption energy of molecules placed perpendicular to the copper (1 1 1) surface is more negative than their parallel state. Also, the 2*H*-form is more stable than the 1*H*-form in both adsorption positions. Tetrazole molecules with electron-donating groups (**2a**, **2b**, **3a**, **3b**, **4a**, and **4b**) have more negative adsorption energy compared to tetrazole molecules (**1a** and **1b**) and tetrazole molecules with electron-withdrawing groups (**5a**, **5b**, **6a**, **6b**, **7a**, and **7b**). For example, in the perpendicular position, the adsorption energy (Table 3), in molecule **3b** (with electron-donating group CH_3O) is equal to −20.2 kcal/mol, and in molecule **6b** (with electron-withdrawing group CN) is equal to −15.3 kcal/mol. Binding energy is classified similarly to

Table 3. Geometrical Parameters of Tetrazole Derivatives after Adsorption on the Cu (1 1 1) Surface[a]

	$\Delta E_{adsorption}$ (kcal/mol)	$\Delta E_{binding}$ (kcal/mol)	Δf_k^+ N2	Δf_k^- N2	Δf_k^+ N3	Δf_k^- N3	Δf_k^+ Cu*	Δf_k^- Cu*	Δq N2	Δq N3	Δq Cu*
					Parallel						
1a	−12.7	12.7	−0.193	−0.169			−0.008	−0.011	0.003		0.013
1b	−12.8	12.8			−0.195	−0.166	−0.015	−0.008		0.004	0.011
2a	−13.0	13.0	−0.197	−0.163			−0.014	−0.011	0.006		0.035
2b	−13.2	13.2			−0.199	−0.149	−0.010	−0.010		0.007	0.035
3a	−13.6	13.6	−0.200	−0.140			−0.017	−0.011	0.008		0.039
3b	−13.7	13.7			−0.205	−0.135	−0.018	−0.017		0.012	0.021
4a	−14.0	14.0	−0.210	−0.098			−0.008	−0.013	0.018		0.042
4b	−14.1	14.1			−0.214	−0.097	−0.015	−0.013		0.024	0.040
5a	−12.1	12.1	−0.186	−0.180			−0.015	−0.013	−0.010		0.027
5b	−12.3	12.3			−0.191	−0.171	−0.013	−0.013		−0.005	0.041
6a	−10.1	10.1	−0.134	−0.184			−0.014	−0.013	−0.016		0.024
6b	−12.0	12.0			−0.141	−0.181	−0.013	−0.012		−0.015	0.025
7a	−8.5	8.5	−0.093	−0.189			−0.010	−0.010	−0.053		0.004
7b	−9.4	9.4			−0.101	−0.185	−0.009	−0.015		−0.022	0.021
					Perpendicular						
1a	−16.5	16.5	−0.205	−0.187			−0.021	−0.013	0.065		0.015
1b	−17.1	17.1			−0.206	−0.185	−0.035	−0.022		0.069	0.005
2a	−18.4	18.4	−0.211	−0.184			−0.022	−0.012	0.071		0.012
2b	−18.6	18.6			−0.218	−0.168	−0.018	−0.017		0.072	0.004
3a	−19.4	19.4	−0.218	−0.161			−0.018	−0.015	0.073		0.015
3b	−20.2	20.2			−0.219	−0.158	−0.020	−0.015		0.074	0.009
4a	−21.8	21.8	−0.222	−0.131			−0.015	−0.018	0.075		0.016
4b	−22.8	22.8			−0.229	−0.121	−0.017	−0.018		0.077	0.012
5a	−16.0	16.0	−0.193	−0.195			−0.019	−0.015	0.040		0.011
5b	−16.3	16.3			−0.203	−0.191	−0.017	−0.019		0.058	0.008
6a	−15.0	15.0	−0.145	−0.197			−0.024	−0.013	0.037		0.004
6b	−15.3	15.3			−0.160	−0.196	−0.017	−0.019		0.039	0.006
7a	−14.3	14.3	−0.113	−0.206			−0.020	−0.018	0.029		0.002
7b	−14.7	14.7			−0.126	−0.198	−0.025	−0.013		0.031	0.001

[a] $\Delta q = q$ (after adsorption) − q (before adsorption), $\Delta f_k^{\pm} = f_k^{\pm}$ (after adsorption) − $f_k^{\pm}$ (before adsorption).

adsorption energy. Therefore, in the optimized states where the adsorption energy and the binding energy have a larger absolute value, they are more effective against copper surface corrosion. According to the data in Table 3, the binding energy for molecule **4b**, which has an electron-donating OH group in the form of 2*H*-tetrazole, is in the perpendicular position of 22.8 kcal/mol, and this value is the most stable compared to the rest.

One of the tools for studying and checking the correlation between different substituents and the nature of the interaction of molecules is to use the Hammett equation. In Figure 5, the adsorption energy graphs are drawn in terms of the para substitution (δ_p) constant for tetrazole molecules and their derivatives that are adsorbed perpendicular and parallel to the copper (1 1 1) surface. As can be seen, for all cases, the regression coefficient (R^2) is greater than 0.7, which indicates a good correlation with the Hammett equation.[71]

3.2.2. Geometrical Parameter Study. Adsorption of tetrazole isomers in parallel and perpendicular modes on the copper surfaces caused some geometrical changes in rings. According to Table 4, which presents the essential geometrical parameters of tetrazole derivatives adsorbed on the copper surface, for the NO_2 and CH_3O substituents, the N1−N2 bond length was obtained 1.357 and 1.366 Å, in parallel configuration, while for the perpendicular mode were 1.350 and 1.363 Å for the **7a** and **3a** isomers, respectively. These values for the **b** isomers were 1.330 and 1.346 Å (in the

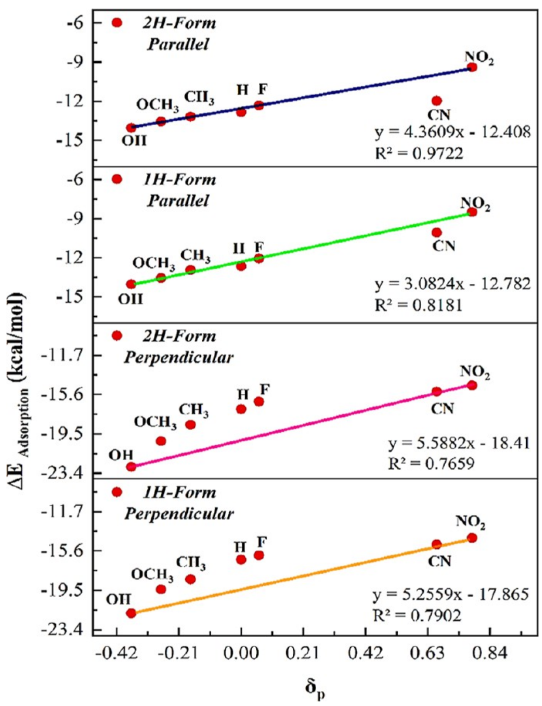

Figure 5. Graphs of adsorption energy in terms of para substitution for different functional groups in tetrazole molecules.

https://doi.org/10.1021/acsomega.2c07185
ACS Omega 2023, 8, 9978−9994

Table 4. Important Geometrical Parameters of Tetrazole Derivatives after Adsorption on the Cu (1 1 1) Surface

	N1−N2	N2−N3	N3−N4	N1−C5	N4−C5	N1−H	N2−H	N2−Cu*	N3−Cu*
					Parallel				
1a	1.358	1.300	1.365	1.347	1.324	1.016		3.244	
1b	1.331	1.338	1.319	1.336	1.357		1.018		3.168
2a	1.358	1.306	1.359	1.353	1.330	1.018		2.788	
2b	1.346	1.346	1.347	1.335	1.363		1.019		2.556
3a	1.366	1.311	1.361	1.355	1.327	1.020		2.594	
3b	1.346	1.346	1.347	1.335	1.363		1.019		2.461
4a	1.367	1.300	1.364	1.348	1.324	1.018		2.362	
4b	1.338	1.336	1.330	1.338	1.354		1.019		2.229
5a	1.363	1.312	1.365	1.349	1.310	1.018		3.354	
5b	1.335	1.340	1.327	1.329	1.345		1.019		3.277
6a	1.353	1.305	1.352	1.362	1.340	1.019		3.489	
6b	1.326	1.345	1.311	1.347	1.370		1.019		3.336
7a	1.357	1.301	1.359	1.355	1.337	1.016		3.551	
7b	1.330	1.341	1.312	1.345	1.367		1.017		3.382
					Perpendicular				
1a	1.335	1.313	1.349	1.344	1.328	1.029		2.111	
1b	1.326	1.344	1.322	1.339	1.350		1.026		2.092
2a	1.357	1.309	1.349	1.346	1.334	1.030		2.109	
2b	1.327	1.341	1.319	1.343	1.357		1.025		2.089
3a	1.363	1.306	1.356	1.348	1.328	1.027		2.108	
3b	1.335	1.337	1.322	1.342	1.355		1.026		2.086
4a	1.366	1.306	1.354	1.313	1.326	1.029		2.099	
4b	1.331	1.339	1.325	1.342	1.347		1.027		2.080
5a	1.361	1.314	1.355	1.344	1.313	1.029		2.125	
5b	1.331	1.343	1.326	1.332	1.341		1.027		2.114
6a	1.352	1.318	1.334	1.361	1.346	1.025		2.166	
6b	1.322	1.350	1.315	1.350	1.364		1.026		2.121
7a	1.350	1.322	1.337	1.351	1.332	1.023		2.183	
7b	1.325	1.349	1.320	1.351	1.343		1.022		2.173

parallel mode for **7b** and **3b**) and 1.325 and 1.335 Å for the perpendicular mode, respectively. One of the main geometrical parameters which may pertain about the molecular inhabitation of tetrazole derivatives is the N−Cu* distance. The results of calculated N−Cu* bond lengths are presented in Table 4. For the tetrazole derivatives in the parallel mode, the calculated values for the 1*H* and 2*H*-tautomers are in the range of 2.362−3.551 and 2.229−3.382 Å, respectively. The tetrazoles with electron-donating groups lay at the least lengths and in parallel mode. On the other hand, the distances of tetrazole rings from the copper surface are in the range of 2.099−2.183 and 2.080−2.173 Å for the 1*H* and 2*H*-tautomers in the perpendicular mode, respectively. The least distance was observed for the 5-hydroxy tetrazole, indicating the effect of the substituent on adsorption efficiency.

3.2.3. Comparison of Mulliken Charges and Fukui Functions. Electric charges in corrosion inhibitor molecules are one of the most substantial factors which are accountable for the interaction with a metal surface. In Table 3, critical quantum chemical factors dependent on the molecular electronic structures of tetrazole derivatives and metal surface, including the difference between the Mulliken charges (Δq), tendency nucleophilic attack (Δf_k^+), and electrophilic attack (Δf_k^-) before and after the tetrazole adsorption are presented. Through the Mulliken population analysis, information can be obtained about the charge values of the d center in each atom in a molecule. By Mulliken atomic charge analysis, inhibitor adsorption centers and charge distribution in the entire framework of the molecule are estimated. Δq positive for the N2 atom in 1*H*-form and the N3 atom in 2*H*-form (Figures 6 and 7) show that the electron transfer from the inhibitor molecule to the copper surface has occurred. As can be seen from Table 3, Δq has become positive for most of the molecules, which indicates their good effect on surface protection. It should be mentioned that in the molecules **5a**, **5b**, **6a**, **6b**, **7a**, and **7b**, which are placed parallel to the surface, the charge has been transferred from the surface to the inhibitor molecule and Δq has a negative value (respectively, equal to −0.010, −0.005, −0.016, −0.015, −0.053, and −0.022). Also, Δq is higher in molecules with electron-donating groups and in the 2*H*-form. For example, in the perpendicular mode, in the case of **4b** (having an electron-donating OH group), the value of Δq for N3 is 0.077 and for Cu* is 0.012, while in molecule **7b** (having an electron-withdrawing nitro group), these values are equal to 0.031 and 0.001, respectively. Therefore, the electron transfer from the molecule to the surface is better in **4b** than in **7b**.

In the following, we will discuss the Fukui functions. Generally, the larger the Δf_k^+ in the N2 atom for the 1*H*-form and the N3 atom for the 2*H*-form (Figures 6 and 7), the more suitable that molecule is for nucleophilic attacks or, in other words, for surface protection. By transferring the negative charge to N2 in the 1*H*-form and N3 in the 2*H*-form, the electron-donating groups make them good nucleophiles, and conversely, the electron-withdrawing groups increase their electrophile. This fact is evident in the values of $\Delta f_k^\pm$. According to Table 3, for molecules **2a**, **2b**, **3a**, **3b**, **4a**, and **4b** in the perpendicular position, the values of Δf_k^+ are equal to

https://doi.org/10.1021/acsomega.2c07185
ACS Omega 2023, 8, 9978−9994

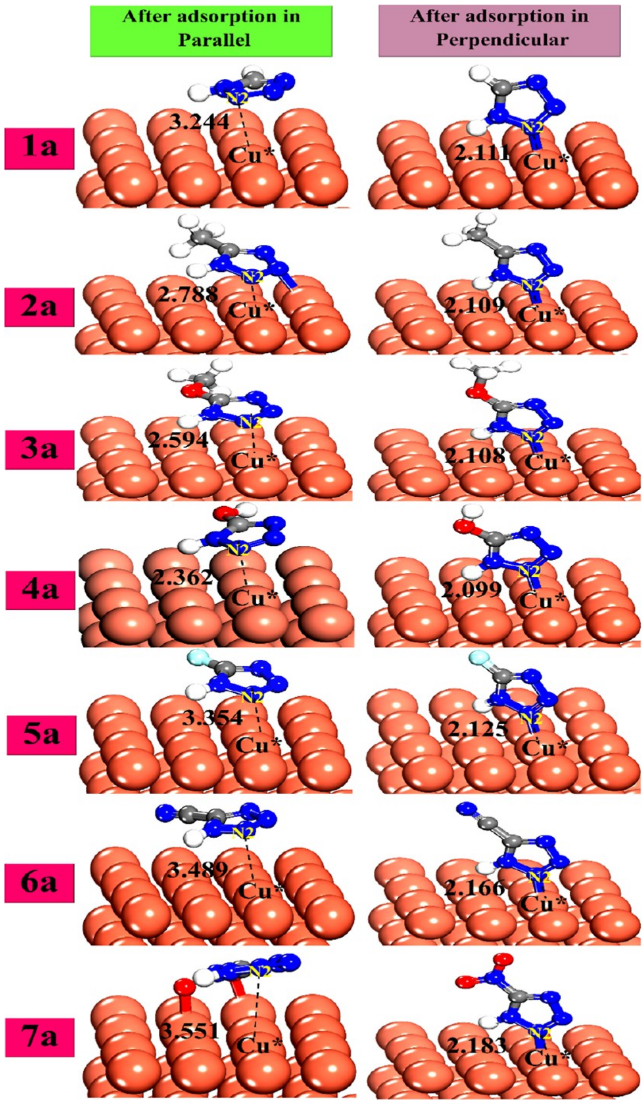

Figure 6. Optimized distances of N2−Cu* in 1*H*-form tetrazole molecules and their derivatives on copper (1 1 1) surface after adsorption in perpendicular and parallel positions.

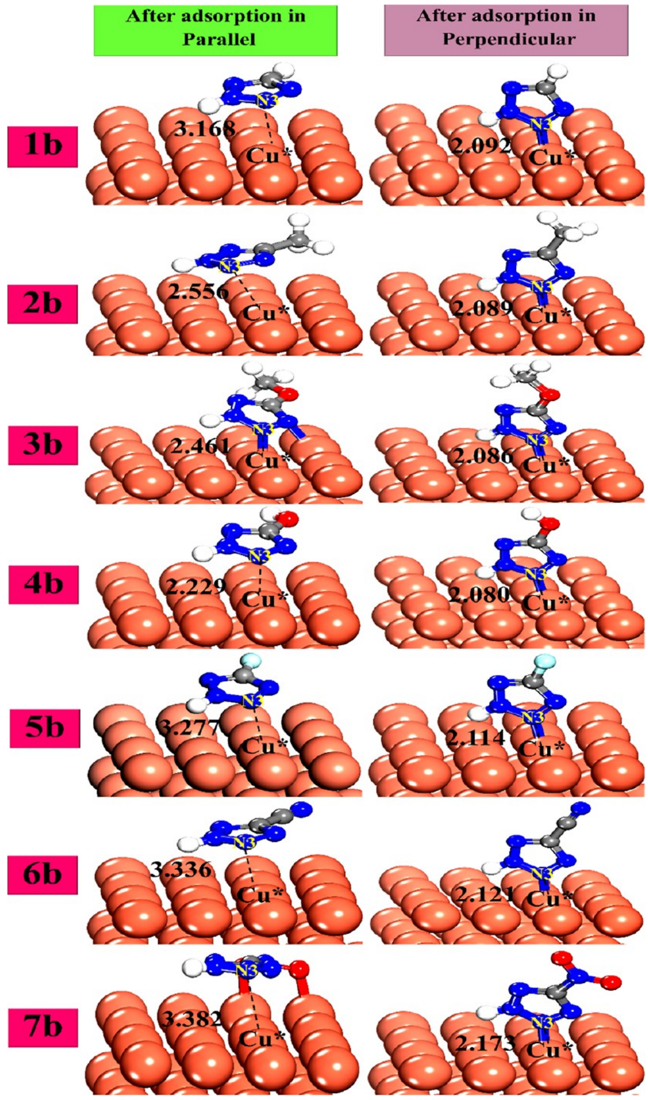

Figure 7. Optimized distances of N3−Cu* in 2*H*-form tetrazole molecules and their derivatives on copper (1 1 1) surface after adsorption in perpendicular and parallel positions.

−0.211, −0.218, −0.218, −0.219, −0.222, and −0.229, and the values of Δf_k^- are equal to −0.184, −0.168, −0.161, −0.158, −0.131, and −0.121. For molecules **5a**, **5b**, **6a**, **6b**, **7a**, and **7b** in the perpendicular position, values of −0.193, −0.203, −0.145, −0.160, −0.113, and −0.126 for Δf_k^+ and values of −0.195, −0.191, −0.197, −0.196, −0.206, and −0.198 for Δf_k^- are observed, respectively. Therefore, in the 2*H*-form molecules with electron-donating groups of CH_3, CH_3O, and OH, we see an increase in Δf_k^+, and in the 2*H*-form molecules with electron-withdrawing groups of F, CN, and NO_2, we also see a decrease in Δf_k^+.

After adsorbing the inhibitory compound, the Cu* atom becomes more negatively charged, its tendency to electrophilic attack decreases and its tendency to nucleophilic attack increases. After the perpendicular adsorption of the 2b molecule on the copper (1 1 1) surface, the values of Δq, Δf_k^+, and Δf_k^- for Cu* are −0.018, −0.017, and 0.004, respectively.

3.2.4. Comparison of PDOS Diagrams. In Figure 8, PDOS diagrams related to the 3d orbital of Cu* and 2p orbital for N2 in the 1*H*-form and N3 in the 2*H*-form of tetrazole molecules and their derivatives before and after adsorption are drawn. As can be seen, before the adsorption of the inhibitor molecule, the peaks related to the 2p orbital are sharp, and after that, they are wide. Also, all positive energy peaks have been removed after adsorption, which indicates the interaction of the 2p orbitals of N2 or N3 with the 3d orbital of Cu*. The peaks related to orbital 3d Cu* have also remained almost constant. Also, in these graphs, the Fermi energy level, which is marked with a dashed line, is set to zero, and the energy value is approximately in the range of −25 to +20 electron volts. By examining the PDOS diagrams (Figure 8), it was observed that among molecules **1a** and **1b**, the intensity of the peak of molecule **1b** had decreased more in conditions perpendicular to the copper surface. Also, these changes in tetrazole molecules in the 2*H*-form, which are perpendicular to the copper surface with electron-donating functional groups, are more than electron-withdrawing groups (especially in molecule **4b** with the OH functional group) and therefore have a more effective reaction with the surface.

3.3. MC Simulation Study. The optimized structures of tetrazole molecules and their derivatives on the copper (1 1 1)

https://doi.org/10.1021/acsomega.2c07185
ACS Omega 2023, 8, 9978−9994

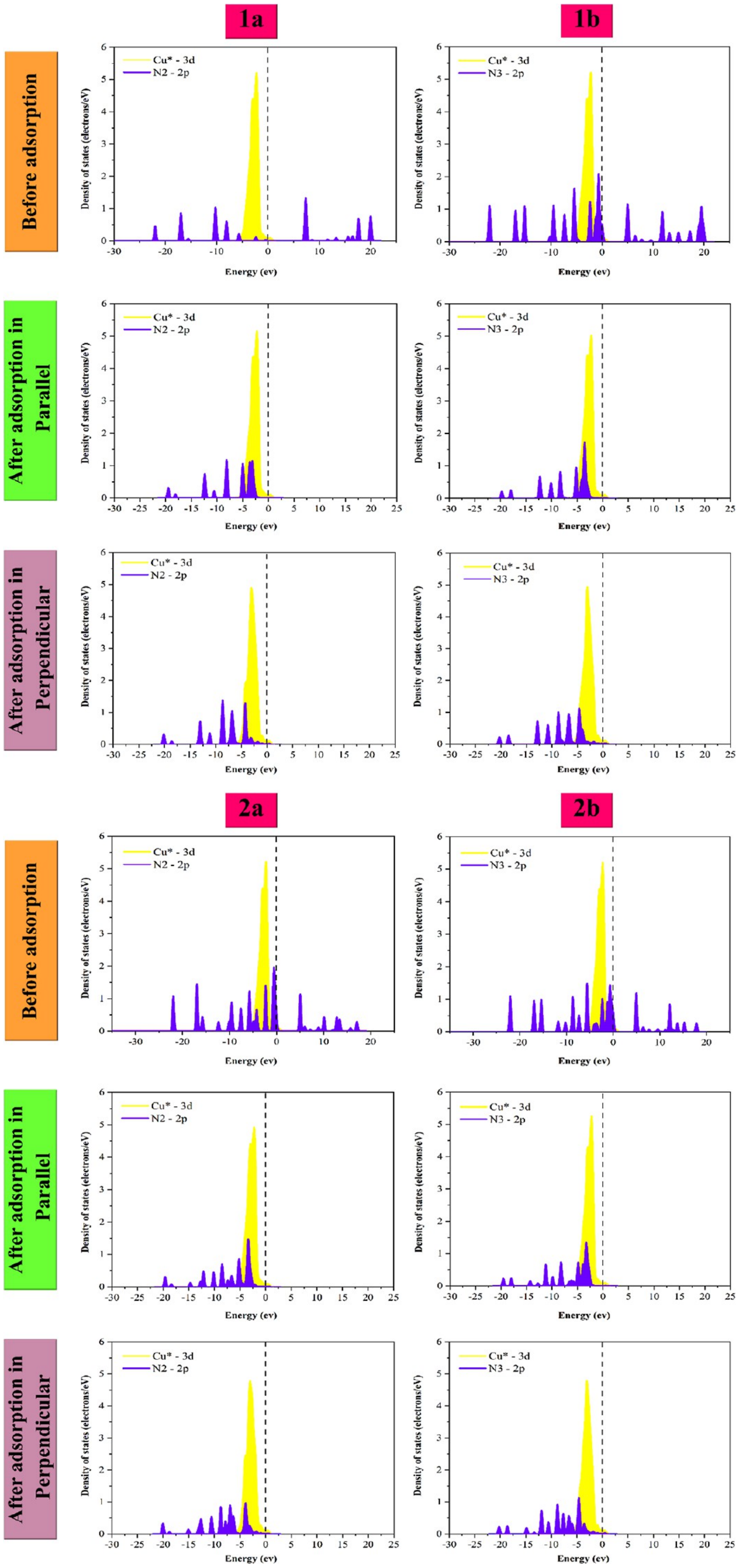

Figure 8. continued

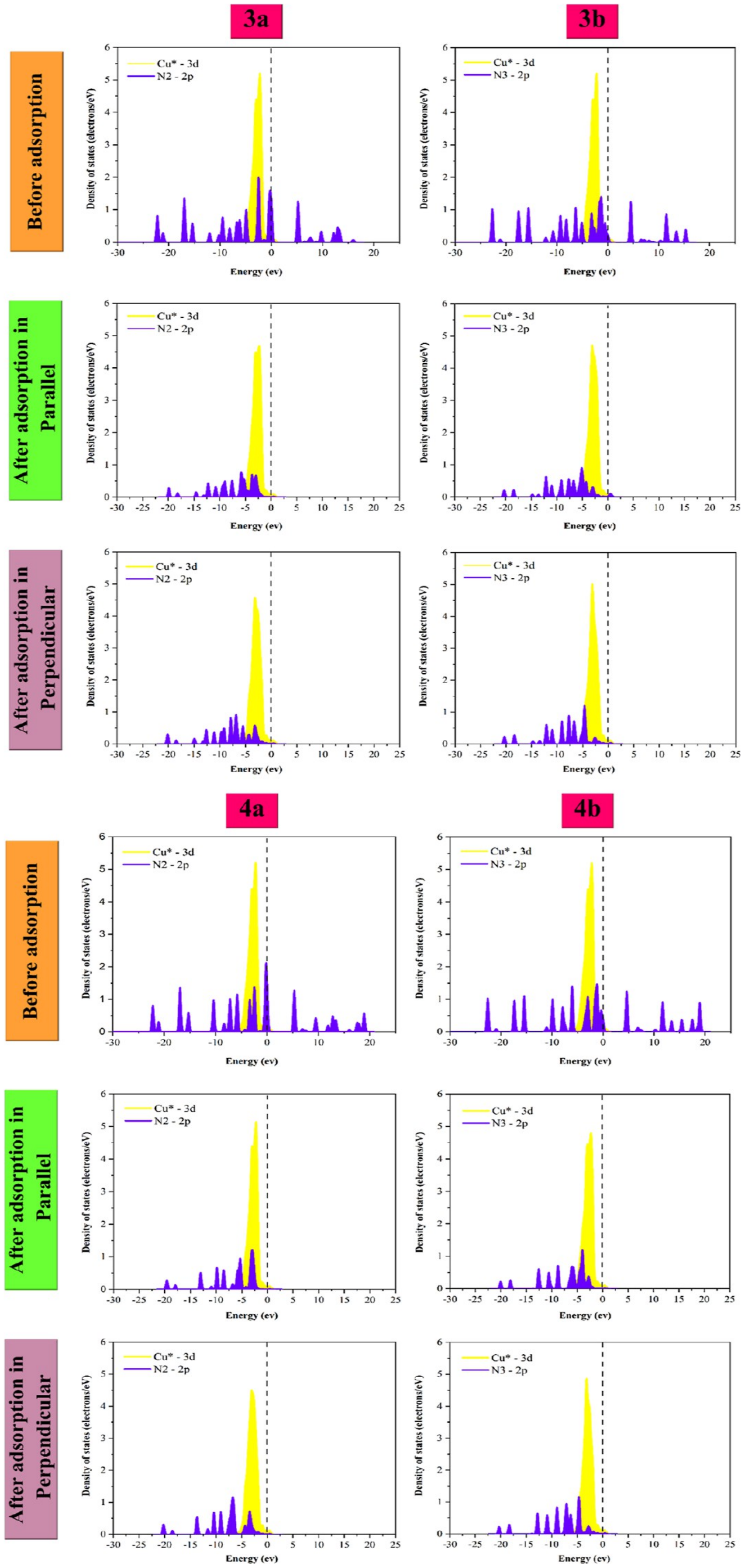

Figure 8. continued

https://doi.org/10.1021/acsomega.2c07185
ACS Omega 2023, 8, 9978−9994

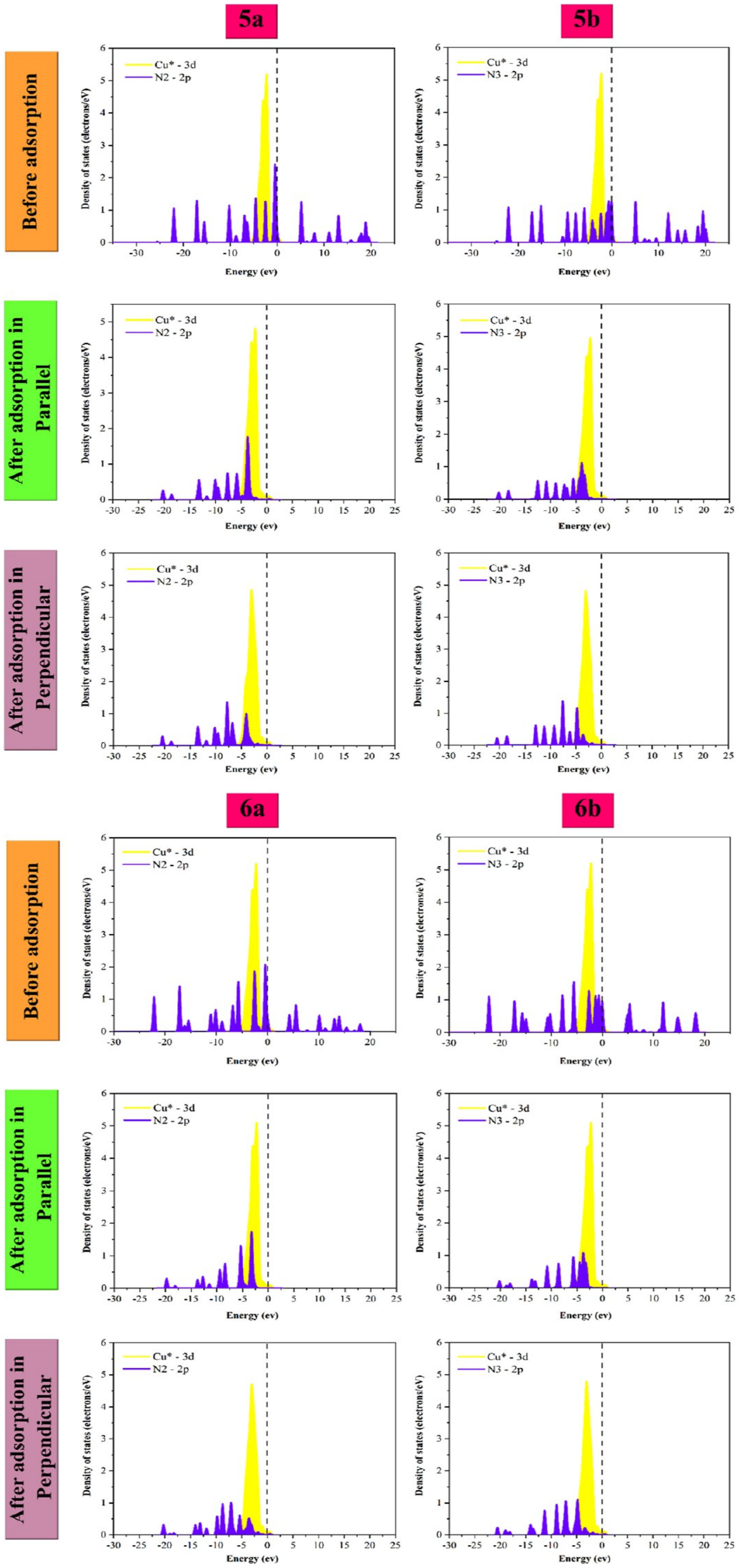

Figure 8. continued

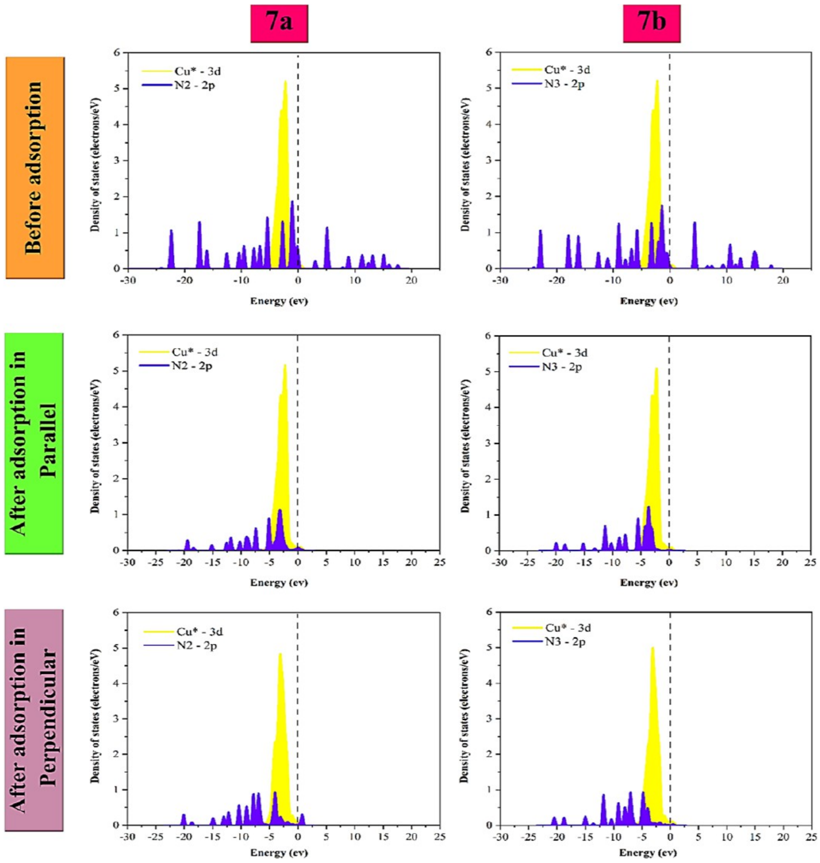

Figure 8. PDOS diagrams related to 2p-N and 3d-Cu* orbitals of tetrazole molecules and their derivatives before adsorption and after adsorption parallel and perpendicular to the copper (1 1 1) surface.

surface, along with 80 water molecules and 2 HCl molecules, are shown in Figure 9. The information obtained from the MC simulation is also listed in Table 5. As seen, in both adsorption modes (perpendicular and parallel), the absolute value of the adsorption energy of inhibitor molecules is higher than the adsorption energy of water and HCl molecules. Therefore, tetrazole molecules and their derivatives are successful in the adsorption competition on the copper surface. For example, in **1a**, **2a**, and **6a** molecules in parallel, the amounts of adsorption energy are equal to −826.0, −834.7, and −813.5 kcal/mol, respectively, and the amounts of water adsorption energy for them are −10.3, −11.4, and −11.6 kcal/mol, and the values of this parameter for HCl are reported as −6, −7.3, and −3.6 kcal/mol, respectively.

Also, in Table 5, by examining the total energies of tetrazole molecules and their derivatives, the role of each of them in preventing surface corrosion can be compared. For example, in the molecules of **1b**, **4b**, and **7b**, the total energy values are −828.2, −843.1, and −815.3 kcal/mol, respectively, in the state perpendicular to the surface. Therefore, inhibitory molecules with electron-donating groups (CH_3, CH_3O, and OH), which are placed perpendicularly to the Cu (1 1 1) surface, have a greater effect in protecting the surface against corrosion by donating electrons to the d orbital of the copper surface.

3.4. Comparison of Previous Studies with This Project. Considering the importance of protecting the copper surface against corrosion, many theoretical and practical studies have been conducted in this field. In Table 6, the values of absorption energy in previous research are given for comparison with this study. As can be seen, the absolute value of the absorption energy for the studied compounds in the case perpendicular to the copper surface in this project is greater than the others, which indicates a better connection with the surface and more effective protection against corrosion.

In this study, the calculation of various parameters showed that electron transfer to the surface is better in compounds containing electron-donating groups. Also, the adsorption of the inhibitor perpendicular to the copper surface shows a greater ability to transfer electrons from the molecule to the surface. These findings were confirmed by comparing the adsorption energies, reducing the N−Cu* bond length, increasing the amount of negative Mulliken charge in Cu, and reducing its electrophilic character.

4. CONCLUSIONS

In this research, a theoretical investigation was carried out by calculation of quantum chemical parameters, DFT calculations, and MC simulation for the anti-corrosion properties of tetrazole tautomers and their derivatives on the copper (111) surface. Among the different surfaces of copper, a 3 × 3 × 1 supercell was created for copper (1 1 1). MC simulation was also done with 80 H_2O molecules and 2 HCl molecules. These calculations were performed for the electron-donating groups CH_3, CH_3O, and OH, as well as for the electron-withdrawing groups F, CN, and NO_2, in two different configurations of the tetrazole molecule (1*H*- and 2*H*-form), and in the perpendicular and parallel states of the Cu (1 1 1) surface. The results showed that tetrazole molecules and their

https://doi.org/10.1021/acsomega.2c07185
ACS Omega 2023, 8, 9978−9994

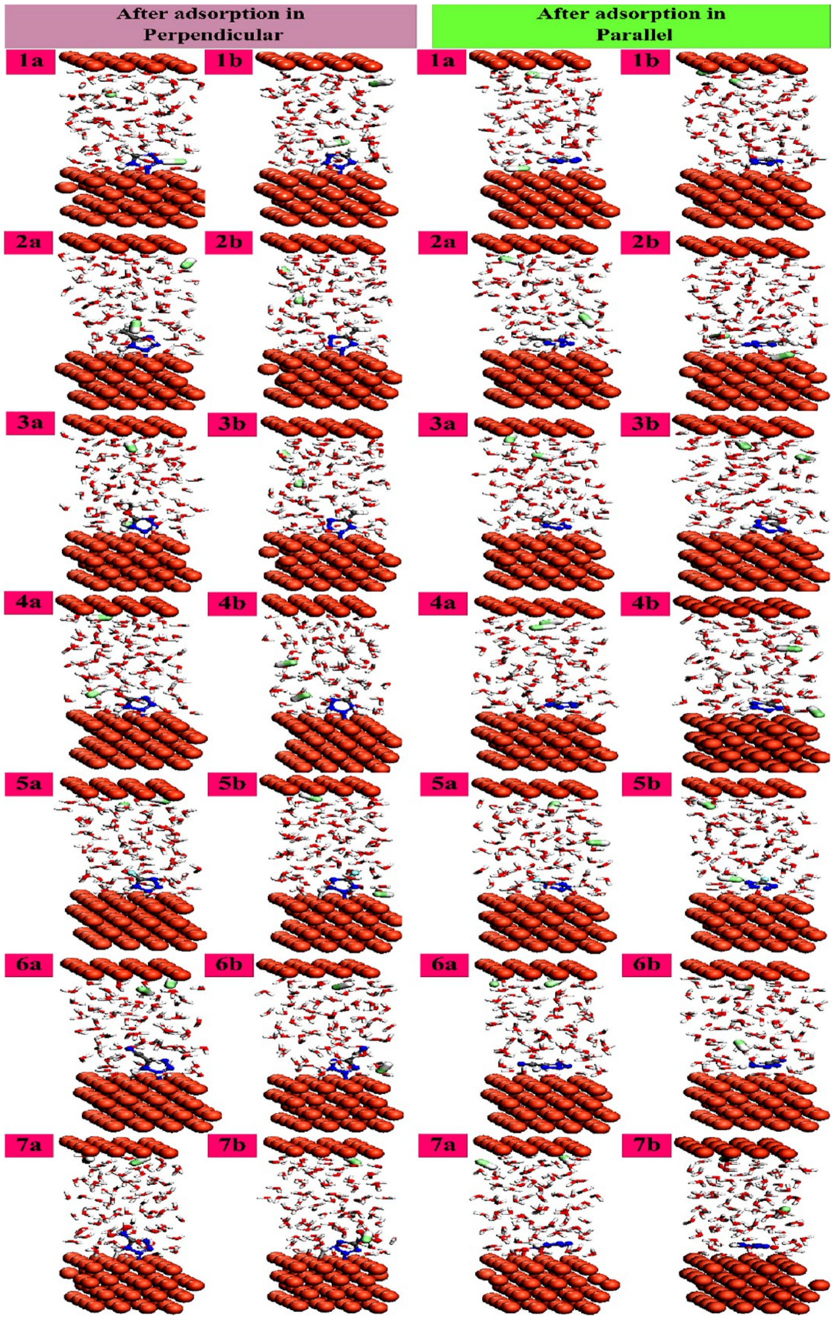

Figure 9. Optimized structures of tetrazole molecules and their derivatives after perpendicular and parallel adsorption on the Cu (1 1 1) surface by MC simulation in the presence of 80 H_2O molecules and 2 HCl molecules.

derivatives having negative and larger adsorption energies than H_2O and HCl can be used as corrosion inhibitors to protect copper surfaces. In this process, by transferring electrons from anti-corrosion compounds to the copper atom, or in other words, by compensating for the lack of electrons in the copper atom, protection against corrosion is created by inhibitory molecules. Also, molecules with electron-donating groups in the form of 2*H* isomers and perpendicular to the surface (especially, the 5-hydroxy-2*H*-tetrazole molecule with absorption energies equal to −22.8 and −860.6 kcal/mol, respectively, in the gas phase and in 2% hydrochloride solution) have a better performance against corrosion. They show copper. Also, the analysis of PDOS, Mulliken charges, Fukui function, geometric parameters, and MC simulation confirm these findings. These results can help researchers in designing and synthesizing more effective molecules in corrosion protection. We hope that the experimental investigation of this process and its comparison with the theoretical results obtained in this work will be done in the future. In addition, the coverage-dependent feature of the inter-adsorption interaction should be calculated by performing calculations with the help of CASTEP tool to investigate the formation of periodic structures or islands on Cu (1 1 1) and the strength of inter-adsorption interactions. Also, on other surfaces of copper and most supercells, and with the help of MC simulation in solutions with higher concentrations, the anti-corrosion properties of these compounds should be investigated.

https://doi.org/10.1021/acsomega.2c07185
ACS Omega 2023, 8, 9978−9994

Table 5. Data from MC Simulation in the Presence of 80 H_2O Molecules and 2 HCl Molecules

	total energy (kcal/mol)	adsorption energy (kcal/mol)	rigid adsorption energy (kcal/mol)	deformation energy (kcal/mol)	dE_{ads}/dN_i water (kcal/mol)	dE_{ads}/dN_i HCl (kcal/mol)
			Parallel			
1a	−808.5	−826.0	−876.0	50.0	−10.3	−6.0
1b	−813.1	−830.6	−881.3	50.7	−11.2	−5.9
2a	−817.2	−834.7	−885.9	51.3	−11.4	−7.3
2b	−820.1	−837.6	−888.6	51.0	−10.2	−4.7
3a	−820.4	−837.9	−888.6	50.6	−13.1	−2.4
3b	−821.0	−838.5	−889.4	51.0	−12.0	−4.4
4a	−836.1	−853.6	−903.8	50.1	−12.7	−6.2
4b	−838.4	−855.9	−905.9	50.0	−13.1	−5.4
5a	−799.6	−817.1	−867.2	50.1	−10.2	−7.5
5b	−806.5	−824.0	−872.1	48.2	−12.3	−3.4
6a	−796.0	−813.5	−863.8	50.3	−11.6	−3.6
6b	−797.1	−814.7	−865.3	50.7	−11.9	−4.6
7a	−797.1	−814.7	−865.3	50.7	−11.9	−4.6
7b	−794.7	−812.2	−862.1	49.8	−9.0	−4.6
			Perpendicular			
1a	−826.2	−843.7	−893.9	50.2	−12.5	−3.1
1b	−828.2	−845.7	−896.2	50.5	−12.2	−7.5
2a	−830.2	−847.7	−898.4	50.7	−12.6	−6.1
2b	−832.6	−850.1	−899.3	49.2	−12.9	−7.0
3a	−833.1	−850.6	−900.4	49.7	−12.7	−6.3
3b	−833.9	−851.5	−900.4	48.9	−13.0	−6.6
4a	−838.8	−856.3	−905.7	49.3	−13.0	−4.5
4b	−843.1	−860.6	−910.8	50.2	−13.3	−3.8
5a	−822.3	−839.8	−890.1	50.3	−11.1	−3.6
5b	−826.2	−843.7	−894.4	50.7	−13.0	−4.9
6a	−817.2	−834.7	−885.9	51.3	−11.4	−7.3
6b	−817.7	−835.2	−885.6	50.4	−12.2	−7.3
7a	−804.9	−822.5	−873.3	50.9	−12.3	−5.0
7b	−815.3	−832.8	−884.7	52.0	−11.9	−4.6

Table 6. Comparison of Adsorption Energy of Previous Studies with This Project

		adsorption energy (kcal/mol)	
	compound	parallel	perpendicular
Kumar.et al.[41]	imidazole	−11.9	−14.0
	purine	−16.6	−16.8
	adenine	−21.6	−17.9
Tan.et al.[37]	PT	−14.5	−15.9
	5-2-BPT	−16.6	−16.8
	5-4-BPT	−14.9	−16.3
Kovačević and Kokalj[40]	imidazole		−15.9
	triazole		−12.68
	tetrazole		−9.91
	pentazole		−5.07
Kokalj.et al.[69]	ATA		−13.8
	BTAH	−16.6	−9.2
	BTAOH	−22.3	−10.6
this study	**1a**	−12.7	−16.5
	1b	−12.8	−17.1
	2a	−13.0	−18.4
	2b	−13.2	−18.6
	3a	−13.6	−19.4
	3b	−13.7	−20.2
	4a	−14.0	−21.8
	4b	−14.1	−22.8

■ AUTHOR INFORMATION

Corresponding Author

Alireza Najafi Chermahini − *Department of Chemistry, Isfahan University of Technology (IUT), Isfahan 8415683111, Iran;* orcid.org/0000-0001-9803-7837; Email: anajafi@iut.ac.ir

Author

Marzieh Esmaeilzadeh Khabazi − *Department of Chemistry, Isfahan University of Technology (IUT), Isfahan 8415683111, Iran;* orcid.org/0000-0003-2562-3012

Complete contact information is available at: https://pubs.acs.org/10.1021/acsomega.2c07185

Notes

The authors declare no competing financial interest.

■ ACKNOWLEDGMENTS

The authors appreciate the support of the Isfahan University of Technology and especially its Chemistry Faculty.

■ REFERENCES

(1) Makar, A. B.; McMartin, K. E.; Palese, M.; Tephly, T. R. Formate Assay in Body Fluids: Application in Methanol Poisoning. *Biochem. Med.* **1975**, *13*, 117−126.

(2) Oukhrib, R.; Abdellaoui, Y.; Berisha, A.; Abou Oualid, H.; Halili, J.; Jusufi, K.; Ait El Had, M.; Bourzi, H.; El Issami, S.; Asmary, F. A.; Parmar, V. S.; Len, C. DFT, Monte Carlo and molecular dynamics simulations for the prediction of corrosion inhibition

efficiency of novel pyrazolylnucleosides on Cu(111) surface in acidic media. *Sci. Rep.* **2021**, *11*, 3771.
(3) Petrović Mihajlović, M. B.; Radovanović, M. B.; Tasić, Ž. Z.; Antonijević, M. M. Imidazole Based Compounds as Copper Corrosion Inhibitors in Seawater. *J. Mol. Liq.* **2017**, *225*, 127−136.
(4) Habib, K. In-Situ Monitoring of Pitting Corrosion of Copper Alloys by Holographic Interferometry. *Corros. Sci.* **1998**, *40*, 1435−1440.
(5) Li, X.; Wan, J.; Ma, Y.; Wang, Y.; Li, X. Study on Cobalt-Phosphate (Co-Pi) Modified BiVO4/Cu2O Photoanode to Significantly Inhibit Photochemical Corrosion and Improve the Photoelectrochemical Performance. *Chem. Eng. J.* **2021**, *404*, 127054.
(6) Hsissou, R.; Abbout, S.; Seghiri, R.; Rehioui, M.; Berisha, A.; Erramli, H.; Assouag, M.; Elharfi, A. Evaluation of Corrosion Inhibition Performance of Phosphorus Polymer for Carbon Steel in [1 M] HCl: Computational Studies (DFT, MC and MD Simulations). *J. Mater. Res. Technol.* **2020**, *9*, 2691−2703.
(7) Desai, M. N. Corrosion inhibitors for copper. *Mater. Corros.* **1972**, *23*, 483−487.
(8) Singh, A. *Corrosion Inhibitors*; IntechOpen, 2019.
(9) Gustinčič, D.; Kokalj, A. A DFT Study of Adsorption of Imidazole, Triazole, and Tetrazole on Oxidized Copper Surfaces: $Cu_2O(111)$ and $Cu_2O(111)$-w/o-Cu^{CUS}. *Phys. Chem. Chem. Phys.* **2015**, *17*, 28602−28615.
(10) Murumkar, P. R.; Ghuge, R. B. Vicinal Diaryl Oxadiazoles, Oxazoles, and Isoxazoles. *Vicinal Diaryl Substituted Heterocycles*; Elsevier, 2018; pp 277−303.
(11) Faisal, M.; Saeed, A.; Shahzad, D.; Abbas, N.; Ali Larik, F.; Ali Channar, P.; Abdul Fattah, T.; Muhammad Khan, D.; Aaliya Shehzadi, S. General Properties and Comparison of the Corrosion Inhibition Efficiencies of the Triazole Derivatives for Mild Steel. *Corros. Rev.* **2018**, *36*, 507−545.
(12) El Ibrahimi, B.; Guo, L. Azole-Based Compounds as Corrosion Inhibitors for Metallic Materials. *Azoles—Synthesis, Properties, Applications and Perspectives*; Kuznetsov, A., Ed.; IntechOpen, 2021
(13) El-Hendawy, M. M.; Kamel, A. M.; Mohamed, M. M. A. The Anti-Corrosive Behavior of Benzo-Fused N-Heterocycles: An in Silico Study toward Developing Organic Corrosion Inhibitors. *Phys. Chem. Chem. Phys.* **2022**, *24*, 743−756.
(14) Wang, H.; Hao, Y.; Chen, S.; Cheng, M.; Li, C.; Sun, S.; Hu, S. DFT Study of Imidazoles Adsorption on the Grain Boundary of Cu (100) Surface. *Corros. Sci.* **2018**, *137*, 33−42.
(15) Vernack, E.; Costa, D.; Tingaut, P.; Marcus, P. DFT Studies of 2-Mercaptobenzothiazole and 2-Mercaptobenzimidazole as Corrosion Inhibitors for Copper. *Corros. Sci.* **2020**, *174*, 108840.
(16) Kiselev, V. G.; Cheblakov, P. B.; Gritsan, N. P. Tautomerism and Thermal Decomposition of Tetrazole: High-Level Ab Initio Study. *J. Phys. Chem. A* **2011**, *115*, 1743−1753.
(17) Allen, F. H.; Groom, C. R.; Liebeschuetz, J. W.; Bardwell, D. A.; Olsson, T. S. G.; Wood, P. A. The Hydrogen Bond Environments of 1*H*-Tetrazole and Tetrazolate Rings: The Structural Basis for Tetrazole-Carboxylic Acid Bioisosterism. *J. Chem. Inf. Model.* **2012**, *52*, 857−866.
(18) Leyva-Ramos, S.; Cardoso-Ortiz, J. Recent Developments in the Synthesis of Tetrazoles and Their Pharmacological Relevance. *Curr. Org. Chem.* **2021**, *25*, 388−403.
(19) Aziz, H.; Saeed, A.; Jabeen, F.; Din, N.; Flörke, U. Synthesis, Single Crystal Analysis, Biological and Docking Evaluation of Tetrazole Derivatives. *Heliyon* **2018**, *4*, No. e00792.
(20) Szatylowicz, H.; Jezuita, A.; Krygowski, T. M. On the Relations between Aromaticity and Substituent Effect. *Struct. Chem.* **2019**, *30*, 1529−1548.
(21) Safapoor, S.; Dekamin, M. G.; Akbari, A.; Naimi-Jamal, M. R. Synthesis of (*E*)-2-(1*H*-Tetrazole-5-yl)-3-Phenylacrylenenitrile Derivatives Catalyzed by New ZnO Nanoparticles Embedded in a Thermally Stable Magnetic Periodic Mesoporous Organosilica under Green Conditions. *Sci. Rep.* **2022**, *12*, 10723.
(22) Koguro, K.; Oga, T.; Mitsui, S.; Orita, R. Novel Synthesis of 5-Substituted Tetrazoles from Nitriles. *Synthesis* **1998**, *1998*, 910−914.
(23) Cao, C.-Y.; Lu, S.; Zhang, D.; Gong, L.-L.; Zhang, H.-P. Effects of Nitroguanidine on the Thermal Behavior and Burning Characteristics of 5-Amino-1*H*-Tetrazole-Based Propellants. *RSC Adv.* **2017**, *7*, 13808−13816.
(24) Wei, C.-X.; Bian, M.; Gong, G.-H. Tetrazolium Compounds: Synthesis and Applications in Medicine. *Molecules* **2015**, *20*, 5528−5553.
(25) da Silva, L.; Sánchez, M.; Ibarra-Rodriguez, M.; Freeman, H. S. Isomeric Tetrazole-Based Organic Dyes for Dye-Sensitized Solar Cells: Structure-Property Relationships. *J. Mol. Struct.* **2022**, *1250*, 131749.
(26) Jafari Chermahini, Z.; Najafi Chermahini, A.; Dabbagh, H. A.; Rezaei, B.; Irannejad, N. The Effects of Second Electron Acceptor Group on the Performance of Tetrazole-Based Nanocrystalline TiO_2 Sensitizers in DSSCs. *Spectrochim. Acta, Part A* **2017**, *178*, 79−85.
(27) Upadhayaya, R. S.; Jain, S.; Sinha, N.; Kishore, N.; Chandra, R.; Arora, S. K. Synthesis of Novel Substituted Tetrazoles Having Antifungal Activity. *Eur. J. Med. Chem.* **2004**, *39*, 579−592.
(28) Monk, B. C.; Keniya, M. V.; Sabherwal, M.; Wilson, R. K.; Graham, D. O.; Hassan, H. F.; Chen, D.; Tyndall, J. D. A. Azole Resistance Reduces Susceptibility to the Tetrazole Antifungal VT-1161. *Antimicrob. Agents Chemother.* **2019**, *63*, e02114−e02118.
(29) Liu, L.; Su, H.; Xing, J.; Peng, D.; Zhang, Q.; Qian, J. Corrosion Inhibition and Friction-Reduction Property of Tetrazole Derivatives on Copper. *Anti-Corros. Methods Mater.* **2018**, *65*, 361−367.
(30) Shaban, M. M.; Negm, N. A.; Farag, R. K.; Fadda, A. A.; Gomaa, A. E.; Farag, A. A.; Migahed, M. A. Anti-Corrosion, Antiscalant and Anti-Microbial Performance of Some Synthesized Trimeric Cationic Imidazolium Salts in Oilfield Applications. *J. Mol. Liq.* **2022**, *351*, 118610.
(31) Qiang, Y.; Li, H.; Lan, X. Self-Assembling Anchored Film Basing on Two Tetrazole Derivatives for Application to Protect Copper in Sulfuric Acid Environment. *J. Mater. Sci. Technol.* **2020**, *52*, 63−71.
(32) Ebenso, E. E.; Verma, C.; Olasunkanmi, L. O.; Akpan, E. D.; Verma, D. K.; Lgaz, H.; Guo, L.; Kaya, S.; Quraishi, M. A. Molecular Modelling of Compounds Used for Corrosion Inhibition Studies: A Review. *Phys. Chem. Chem. Phys.* **2021**, *23*, 19987−20027.
(33) Abderrahim, K.; Khamaysa, O. M. A.; Selatnia, I.; Zeghache, H. Adsorption and Performance Assessment of 5-Mercapto-1-Methyl Tetrazole as A9M Steel Corrosion Inhibitor in HCl Medium: A Detailed Experimental, and Computational Methods. *Chemical Data Collections* **2022**, *39*, 100848.
(34) Qiang, Y.; Zhi, H.; Guo, L.; Fu, A.; Xiang, T.; Jin, Y. Experimental and Molecular Modeling Studies of Multi-Active Tetrazole Derivative Bearing Sulfur Linker for Protecting Steel from Corrosion. *J. Mol. Liq.* **2022**, *351*, 118638.
(35) Mahmmod, A. A.; Kazarinov, I. A.; Khadom, A. A.; Mahood, H. B. Experimental and Theoretical Studies of Mild Steel Corrosion Inhibition in Phosphoric Acid Using Tetrazoles Derivatives. *J. Bio. Tribo. Corros.* **2018**, *4*, 58.
(36) Bourzi, H.; Oukhrib, R.; Ibrahimi, B. E.; Oualid, H. A.; Abdellaoui, Y.; Balkard, B.; Hilali, M.; Issami, S. E. Understanding of Anti-Corrosive Behavior of Some Tetrazole Derivatives in Acidic Medium: Adsorption on Cu (111) Surface Using Quantum Chemical Calculations and Monte Carlo Simulations. *Surf. Sci.* **2020**, *702*, 121692.
(37) Tan, B.; Zhang, S.; Liu, H.; Qiang, Y.; Li, W.; Guo, L.; Chen, S. Insights into the Inhibition Mechanism of Three 5-Phenyltetrazole Derivatives for Copper Corrosion in Sulfuric Acid Medium via Experimental and DFT Methods. *J. Taiwan Inst. Chem. Eng.* **2019**, *102*, 424−437.
(38) Chiter, F.; Costa, D.; Maurice, V.; Marcus, P. DFT Investigation of 2-Mercaptobenzothiazole Adsorption on Model Oxidized Copper Surfaces and Relationship with Corrosion Inhibition. *Appl. Surf. Sci.* **2021**, *537*, 147802.
(39) Liu, P.; Fang, X.; Tang, Y.; Sun, C.; Yao, C. Electrochemical and Quantum Chemical Studies of 5-Substituted Tetrazoles as

Corrosion Inhibitors for Copper in Aerated 0.5 M H_2SO_4 Solution. *Mater. Sci. Appl.* **2011**, *02*, 1268−1278.

(40) Kovačević, N.; Kokalj, A. DFT Study of Interaction of Azoles with Cu (111) and Al (111) Surfaces: Role of Azole Nitrogen Atoms and Dipole−Dipole Interactions. *J. Phys. Chem. C* **2011**, *115*, 24189−24197.

(41) Kumar, D.; Jain, V.; Rai, B. Imidazole Derivatives as Corrosion Inhibitors for Copper: A DFT and Reactive Force Field Study. *Corros. Sci.* **2020**, *171*, 108724.

(42) Kumar, D.; Jain, V.; Rai, B. Capturing the Synergistic Effects between Corrosion Inhibitor Molecules Using Density Functional Theory and ReaxFF Simulations—A Case for Benzyl Azide and Butyn-1-Ol on Cu Surface. *Corros. Sci.* **2022**, *195*, 109960.

(43) Najafi Chermahini, A.; Nasr-Esfahani, M.; Dalirnasab, Z.; Dabbagh, H. A.; Teimouri, A. Theoretical Studies on Tautomerism of Tetrazole Derivatives by Polarisable Continuum Method (PCM). *J. Mol. Struct.* **2007**, *820*, 7−11.

(44) Chermahini, A. N.; Teimouri, A.; Beni, A. S. Theoretical Studies on Tautomerism of Tetrazole 5-Thion. *Struct. Chem.* **2011**, *22*, 175−181.

(45) Chermahini, A. N.; Ghaedi, A.; Teimouri, A.; Momenbeik, F.; Dabbagh, H. A. Density Functional Theory Study of Intermolecular Interactions of Cyclic Tetrazole Dimers. *J. Mol. Struct.* **2008**, *867*, 78−84.

(46) Najafi Chermahini, A.; Dabbagh, H. A.; Teimouri, A. Relation between the Substituent Effect and Aromaticity in Tetrazoles, Protonated Tetrazoles and Tetrazolate Derivatives. *J. Mol. Struct.* **2007**, *822*, 33−37.

(47) Wang, H.; Wang, X.; Wang, H.; Wang, L.; Liu, A. DFT Study of New Bipyrazole Derivatives and Their Potential Activity as Corrosion Inhibitors. *J. Mol. Model.* **2006**, *13*, 147−153.

(48) Valiev, M.; Bylaska, E. J.; Govind, N.; Kowalski, K.; Straatsma, T. P.; Van Dam, H. J. J.; Wang, D.; Nieplocha, J.; Apra, E.; Windus, T. L.; de Jong, W. A. NWChem: A Comprehensive and Scalable Open-Source Solution for Large Scale Molecular Simulations. *Comput. Phys. Commun.* **2010**, *181*, 1477−1489.

(49) Saha, S. Kr.; Ghosh, P.; Hens, A.; Murmu, N. C.; Banerjee, P. Density Functional Theory and Molecular Dynamics Simulation Study on Corrosion Inhibition Performance of Mild Steel by Mercapto-Quinoline Schiff Base Corrosion Inhibitor. *Phys. E Low-dimens. Syst. Nanostruct.* **2015**, *66*, 332−341.

(50) Lee, C.; Yang, W.; Parr, R. G. Development of the Colle-Salvetti Correlation-Energy Formula into a Functional of the Electron Density. *Phys. Rev. B* **1988**, *37*, 785−789.

(51) Madkour, L. H.; Kaya, S.; Obot, I. B. Computational, Monte Carlo Simulation and Experimental Studies of Some Arylazotriazoles (AATR) and Their Copper Complexes in Corrosion Inhibition Process. *J. Mol. Liq.* **2018**, *260*, 351−374.

(52) Hadisaputra, S.; Purwoko, A. A.; Hakim, A.; Prasetyo, N.; Hamdiani, S. Corrosion Inhibition Properties of Phenyl Phthalimide Derivatives against Carbon Steel in the Acidic Medium: DFT, MP2, and Monte Carlo Simulation Studies. *ACS Omega* **2022**, *7*, 33054−33066.

(53) Akpan, E. D.; Oladipo, S. D.; Quadri, T. W.; Olasunkanmi, L. O.; Nwanna, E. E.; Omondi, B.; Ebenso, E. E. Formamidine-Based Thiuram Disulfides as Efficient Inhibitors of Acid Corrosion of Mild Steel: Electrochemical, Surface, and Density Functional Theory/Monte Carlo Simulation Studies. *ACS Omega* **2022**, *7*, 26076−26091.

(54) Xu, B.; Ji, Y.; Zhang, X.; Jin, X.; Yang, W.; Chen, Y. Experimental and Theoretical Studies on the Corrosion Inhibition Performance of 4-Amino-N,N-Di-(2-Pyridylmethyl)-Aniline on Mild Steel in Hydrochloric Acid. *RSC Adv.* **2015**, *5*, 56049−56059.

(55) Wong, M. W.; Leung-Toung, R.; Wentrup, C. Tautomeric Equilibrium and Hydrogen Shifts of Tetrazole in the Gas Phase and in Solution. *J. Am. Chem. Soc.* **1993**, *115*, 2465−2472.

(56) Lesar, A.; Milošev, I. Density Functional Study of the Corrosion Inhibition Properties of 1,2,4-Triazole and Its Amino Derivatives. *Chem. Phys. Lett.* **2009**, *483*, 198−203.

(57) Lai, Z.; Wang, S.; Wang, C.; Hong, Y.; Zhou, G.; Chen, Y.; He, W.; Peng, Y.; Xiao, D. A Comparison of Typical Additives for Copper Electroplating Based on Theoretical Computation. *Comput. Mater. Sci.* **2018**, *147*, 95−102.

(58) Cao, Z.; Tang, Y.; Cang, H.; Xu, J.; Lu, G.; Jing, W. Novel Benzimidazole Derivatives as Corrosion Inhibitors of Mild Steel in the Acidic Media. Part II: Theoretical Studies. *Corros. Sci.* **2014**, *83*, 292−298.

(59) Ammouchi, N.; Allal, H.; Belhocine, Y.; Bettaz, S.; Zouaoui, E. DFT Computations and Molecular Dynamics Investigations on Conformers of Some Pyrazinamide Derivatives as Corrosion Inhibitors for Aluminum. *J. Mol. Liq.* **2020**, *300*, 112309.

(60) Gutiérrez, E.; Rodríguez, J. A.; Cruz-Borbolla, J.; Alvarado-Rodríguez, J. G.; Thangarasu, P. Development of a Predictive Model for Corrosion Inhibition of Carbon Steel by Imidazole and Benzimidazole Derivatives. *Corros. Sci.* **2016**, *108*, 23−35.

(61) Oguzie, E. E.; Adindu, C. B.; Enenebeaku, C. K.; Ogukwe, C. E.; Chidiebere, M. A.; Oguzie, K. L. Natural Products for Materials Protection: Mechanism of Corrosion Inhibition of Mild Steel by Acid Extracts of Piper Guineense. *J. Phys. Chem. C* **2012**, *116*, 13603−13615.

(62) Takeuchi, K.; Suda, A.; Ushioda, S. Local Variation of the Work Function of Cu(111) Surface Deduced from the Low Energy Photoemission Spectra. *Surf. Sci.* **2001**, *489*, 100−106.

(63) Farrokhpour, H.; Hadadzadeh, H.; Eskandari, K.; Movahedi, M.; Jouypazadeh, H. Van Der Waals DFT ONIOM Study of the Adsorption of DNA Bases on the Cu(111) Nanosurface. *Appl. Surf. Sci.* **2017**, *422*, 372−387.

(64) Udhayakala, P.; Rajendiran, T. V.; Gunasekaran, S. Theoretical Approach to the Corrosion Inhibition Efficiency of Some Pyrimidine Derivatives Using DFT Method. *J. Comput. Methods Mol. Des.* **2012**, *2*, 1−15.

(65) Fuentealba, P.; Pérez, P.; Contreras, R. On the Condensed Fukui Function. *J. Chem. Phys.* **2000**, *113*, 2544−2551.

(66) Bourzi, H.; Oukhrib, R.; El Ibrahimi, B.; Abou Oualid, H.; Abdellaoui, Y.; Balkard, B.; El Issami, S.; Hilali, M.; Bazzi, L.; Len, C. Furfural Analogs as Sustainable Corrosion Inhibitors-Predictive Efficiency Using DFT and Monte Carlo Simulations on the Cu(111), Fe(110), Al(111) and Sn(111) Surfaces in Acid Media. *Sustainability* **2020**, *12*, 3304.

(67) Kumar, D.; Jain, V.; Rai, B. Unravelling the Mechanisms of Corrosion Inhibition of Iron by Henna Extract: A Density Functional Theory Study. *Corros. Sci.* **2018**, *142*, 102−109.

(68) Guo, L.; Qi, C.; Zheng, X.; Zhang, R.; Shen, X.; Kaya, S. Toward Understanding the Adsorption Mechanism of Large Size Organic Corrosion Inhibitors on an Fe(110) Surface Using the DFTB Method. *RSC Adv.* **2017**, *7*, 29042−29050.

(69) Kokalj, A.; Peljhan, S. Density Functional Theory Study of ATA, BTAH, and BTAOH as Copper Corrosion Inhibitors: Adsorption onto Cu(111) from Gas Phase. *Langmuir* **2010**, *26*, 14582−14593.

(70) Sun, S.; Geng, Y.; Tian, L.; Chen, S.; Yan, Y.; Hu, S. Density Functional Theory Study of Imidazole, Benzimidazole and 2-Mercaptobenzimidazole Adsorption onto Clean Cu(111) Surface. *Corros. Sci.* **2012**, *63*, 140−147.

(71) Hansch, C.; Leo, A.; Taft, R. W. A Survey of Hammett Substituent Constants and Resonance and Field Parameters. *Chem. Rev.* **1991**, *91*, 165−195.

https://doi.org/10.1021/acsomega.2c07185
ACS Omega 2023, 8, 9978−9994